e-ISSN: 2289-649X

Available online at
https://journal.uitm.edu.my/ojs/index.php/SRJ

Scientific Research Journal 23(2) 2026, 151–163

Scientific Research Journal

Sintering Temperature Dependence of Structural and Morphological Properties of $PrMnO_3$ Perovskite Manganite

Muhamad Fauzan Fakhri Mohamad[1,2], Nur Baizura Mohamed[3*], Siti Aishah Abdul Aziz[4], Rozilah Rajmi[5], Zakiah Mohamed[6]

[1,3,4]*Faculty of Applied Sciences, Universiti Teknologi MARA Pahang Branch, Jengka Campus, 26400 Bandar Tun Razak, Jengka, Pahang, Malaysia*
[2]*Infineon Technologies (Malaysia) Sdn. Bhd, Free Trade Zone, Batu Berendam, 75350 Melaka, Malaysia*
[5]*Faculty of Applied Sciences, Universiti Teknologi MARA Perlis Branch, Arau Campus, 02600 Arau, Perlis, Malaysia*
[6]*Faculty of Applied Sciences, Universiti Teknologi MARA, 40450 Shah Alam, Selangor, Malaysia*

ARTICLE INFO

Article history:
Received 13 July 2026
Revised 17 August 2026
Accepted 24 August 2026
Online first
Published 11 September 2026

Keywords:
$PrMnO_3$
Perovskite Manganite Sintering Temperature X-Ray Diffraction Rietveld Refinement SEM-EDX

DOI:

10.24191/srj.v23i2.58611

ABSTRACT

$PrMnO_3$ perovskite manganite ceramics were synthesised using the conventional solid-state reaction method and sintered at 1000 °C, 1050 °C and 1100 °C to investigate the influence of sintering temperature on their structural and morphological properties. X-ray diffraction analysis showed that the main diffraction peaks of all samples correspond to an orthorhombic perovskite-related $PrMnO_3$ structure with *Pnma* symmetry. Rietveld refinement confirmed the orthorhombic lattice and revealed slight variations in lattice parameters, unit-cell volume, Mn-O bond length and Mn-O-Mn bond angle with sintering temperature. The χ^2 value decreased from 1.680 for the sample sintered at 1000 °C to 1.463 for the sample sintered at 1100 °C, while the profile residuals showed some variation among the samples. Weak secondary reflections were observed, but their contribution was reduced with increasing sintering temperature. SEM micrographs showed progressive densification, clearer grain boundaries and reduced intergranular porosity as the sintering temperature increased. EDX analysis confirmed the presence of Pr, Mn and O as the main constituent elements in all samples. Among the investigated temperatures, the sample sintered at 1100 °C showed the most favourable structural and morphological

[3*]Corresponding author. *E-mail address* : nurbaizura620@uitm.edu.my

development, with improved phase formation, lower secondary-phase contribution and denser microstructure. These findings demonstrate the important role of sintering temperature in controlling the structural and morphological characteristics of undoped $PrMnO_3$ ceramics.

1. INTRODUCTION

Perovskite oxides with the general formula ABO_3 have attracted considerable attention due to their flexible crystal structure and tunable physical properties. In this structure, the A-site is commonly occupied by rare-earth or alkaline-earth cations, while B-site is occupied by transition-metal cations surrounded by oxygen octahedra. Among these materials, rare-earth manganites with the general formula $RMnO_3$ are widely studied because of the strong coupling between lattice, charge, spin and orbital degrees of freedom. This coupling gives rise to various structural, electrical and magnetic behaviours that are sensitive to composition, synthesis route and heat-treatment conditions [1-3].

$PrMnO_3$ is an important parent compound in the rare-earth manganite family. It commonly crystallises in a distorted orthorhombic perovskite structure with *Pnma* symmetry, where the distortion is mainly associated with the tilting of MnO_6 octahedra and the size mismatch between the Pr-site cation and the Mn-O framework [1,4]. The parent $PrMnO_3$ system is particularly useful as a structural reference before further modification through doping or substitution. Many reported studies on $PrMnO_3$-based manganites focus on doped systems because cation substitution can modify the Mn^{3+}/Mn^{4+} ratio, oxygen vacancy concentration, lattice distortion and physical response [5,6]. However, understanding the undoped parent compound remains essential because its structural stability, phase formation and microstructure influence the interpretation of any later doped or functional system.

The synthesis condition plays a major role in determining the final properties of perovskite manganite ceramics. In solid-state reaction, sintering temperature is one of the most important parameters because it affects atomic diffusion, reaction completeness, crystallinity, densification and grain growth. Insufficient sintering may lead to incomplete phase formation, residual secondary phases and porous microstructure. On the other hand, higher sintering temperature may improve crystallisation and densification, although excessive heat treatment can also promote secondary phase formation or compositional deviation in some oxide systems [7-9]. Therefore, a systematic evaluation of sintering temperature is necessary to establish suitable processing conditions for undoped $PrMnO_3$ ceramics.

Previous studies have shown that sintering temperature affects the structural and microstructural development of $PrMnO_3$ and related Pr-based manganites, although the reported systems were prepared under different conditions. Keshvani et al. [10] investigated undoped nanostructured $PrMnO_3$ prepared by a modified sol-gel route and sintered between 700 and 1000 °C. The orthorhombic *Pnma* structure was retained, while the crystallite and grain sizes increased with sintering temperature. In comparison, Teoh and Shamsuddin [11] studied solid-state-synthesised Na/Ag-doped Pr-based manganite at 1100-1200 °C and reported the same *Pnma* symmetry together with improved grain connectivity, densification and

https://doi.org/10.24191/srj.v23i2.58611

reduced porosity at higher temperatures. These studies demonstrate the importance of thermal processing, but they involve either a different synthesis route or a chemically substituted Pr-based system. The present study therefore provides a complementary assessment of undoped bulk $PrMnO_3$ prepared by the conventional solid-state route within the intermediate 1000-1100 °C processing window. In particular, the 50 °C intervals allow relatively small changes in phase development, refined crystal structure and microstructure to be examined.

Accordingly, this work investigates the structural and morphological evolution of undoped $PrMnO_3$ ceramics sintered at 1000, 1050 and 1100 °C. The selected temperatures form a controlled post-calcination processing range above the 950 °C calcination stage, while the composition, synthesis route and sintering duration are kept unchanged. XRD and Rietveld refinement are used to evaluate phase formation, lattice parameters, unit-cell volume and Mn-O bond geometry, while SEM and EDX provide complementary information on microstructural development and elemental composition. The weak secondary reflections observed in the diffraction patterns are also examined in relation to sintering temperature.

2. METHODOLOGY

2.1 Sample Preparation

$PrMnO_3$ ceramics were prepared using the conventional solid-state reaction method. High-purity praseodymium oxide, Pr_6O_{11} and manganese oxide, MnO_2, were used as starting materials. The powders were weighed according to the stoichiometric ratio required to form $PrMnO_3$ based on Eq. (1).

$$2Pr_6O_{11} + 12MnO_2 \rightarrow 12PrMnO_3 + 5O_2 \quad (1)$$

For each batch, the calculated masses of Pr_6O_{11} and MnO_2 were 1.9859 and 1.0141 g, respectively, to obtain approximately 3 g of $PrMnO_3$ powder. The powders were thoroughly mixed and ground using an agate mortar and pestle for 2 h to obtain a homogeneous mixture. The mixed powder was then calcined at 950 °C for 24 h in a furnace to promote the initial solid-state reaction.

After calcination, the powder was reground for another 2 h to improve homogeneity. The resulting powder was pressed into pellets with approximately 10 mm diameter and 3 mm thickness using a pellet press under a pressure of 30 MPa. The pellets were then sintered at three different temperatures, namely 1000 °C, 1050 °C and 1100 °C, for 36 h. The heating and cooling rates were maintained at 25 °C/min. The sintered samples were labelled according to their sintering temperatures as P1000, P1050 and P1100, respectively.

2.2 X-Ray Diffraction and Rietveld Refinement

The phase formation and crystal structure of the sintered $PrMnO_3$ ceramics were examined using a PANalytical X'Pert PRO X-ray diffractometer equipped with a Cu X-ray source and an X'Celerator detector. Cu Kα radiation was used with $K\alpha_1$ = 1.540598 Å and $K\alpha_2$ = 1.544426 Å. The X-ray tube operated at 45 kV and 40 mA. Diffraction data were collected at room temperature in continuous mode over approximately 5-90° in 2θ, with a data interval of approximately 0.0167° and a counting time of 1.905 s.

https://doi.org/10.24191/srj.v23i2.58611

The recorded acquisition time corresponds to an effective scan rate of approximately 56° 2θ min^{-1}. The diffraction range from 15-80° was subsequently used for Rietveld refinement and structural analysis.

Rietveld refinement was performed to obtain the refined lattice parameters, unit-cell volume, Mn-O bond length, Mn-O-Mn bond angle and goodness-of-fit values. The refinement was conducted using the General Structure Analysis System (GSAS) with the EXPGUI interface. The refinement reliability was assessed using the profile R factor (R_p), weighted-profile R factor (R_{wp}), expected R factor (R_{exp}), and the chi-square statistic (χ^2). These parameters were considered together to evaluate the agreement between the observed and calculated diffraction profiles [12,13]. The crystal structure visualization was performed using VESTA software. The orthorhombic *Pnma* structure was used as the initial model for the refinement. The observed and calculated diffraction profiles, difference curves, background contribution and Bragg peak positions were compared to evaluate the refinement quality.

2.3 SEM and EDX Analysis

The surface morphology of the sintered $PrMnO_3$ ceramics was examined using a TESCAN VEGA3 SBU scanning electron microscope. The micrographs used in this study were recorded at approximately 3000x magnification using the secondary-electron detector at an accelerating voltage of 20 kV. The SEM observations were used to compare grain morphology, grain connectivity, intergranular porosity and densification with sintering temperature.

Energy dispersive X-ray (EDX) spectroscopy was performed using an Oxford Instruments EDX system with AZtec software to determine the elemental composition of the samples. The EDX spectra were used to confirm Pr, Mn and O as the main constituent elements, while the corresponding weight and atomic percentages were compared among the samples.

3. RESULTS AND DISCUSSION

3.1 XRD Phase Formation

Fig. 1 shows the X-ray diffraction patterns of $PrMnO_3$ ceramics sintered at 1000 °C, 1050 °C and 1100 °C. The main diffraction peaks observed for all samples can be assigned to an orthorhombic perovskite-related $PrMnO_3$ structure with *Pnma* symmetry. This structural symmetry is commonly reported for rare-earth manganite systems, including $PrMnO_3$-based perovskite [1,4,5]. The presence of the main diffraction peaks at similar 2θ positions for all samples indicates that the principal $PrMnO_3$ perovskite framework is retained within the investigated sintering temperature range.

The retention of the *Pnma* structure across the present temperature range is consistent with Keshvani et al. [10], who reported single-phase undoped $PrMnO_3$ prepared by a modified sol-gel route and sintered between 700 and 1000 °C. Their system, however, was nanostructured and prepared by a different synthesis route, whereas the present solid-state ceramics retain weak secondary reflections. This difference suggests that phase development is influenced not only by sintering temperature but also by the synthesis and processing conditions.

https://doi.org/10.24191/srj.v23i2.58611

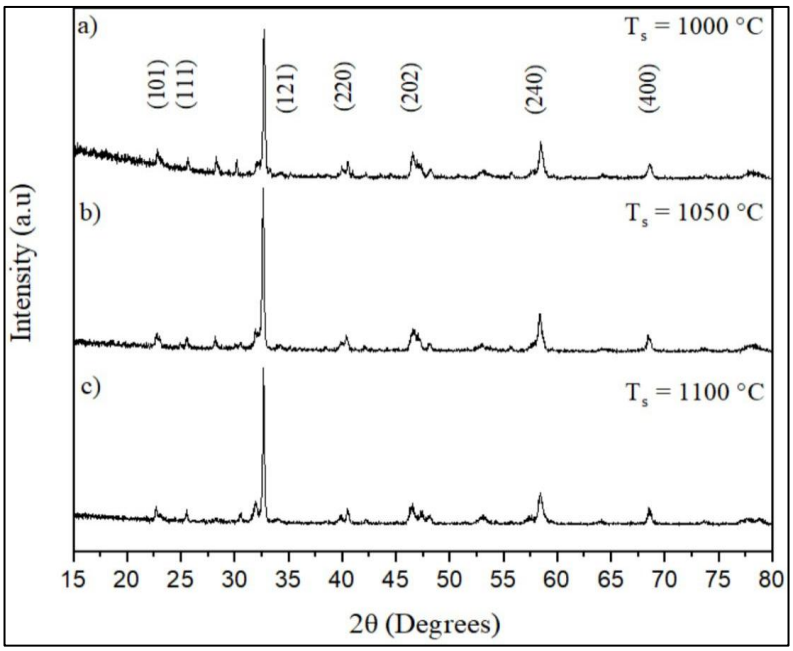

Fig. 1. X-ray diffraction patterns of $PrMnO_3$ ceramics sintered at temperatures, Ts, of (a) 1000 °C, (b) 1050 °C and (c) 1100 °C, showing the formation of an orthorhombic perovskite-related structure with *Pnma* symmetry

The diffraction profiles show a gradual improvement as the sintering temperature increases. The sample sintered at 1000 °C exhibits relatively weaker peak definition together with several small additional reflections. This suggests that the phase development is less complete at the lower sintering temperature. As the sintering temperature increases to 1050 °C and 1100 °C, the diffraction peaks become more distinct, indicating improved crystallinity and better phase formation. This behaviour is consistent with the role of thermal treatment in ceramic oxide synthesis, where higher sintering temperatures promote atomic diffusion, precursor reaction, crystallite growth and phase development [7-9]. Weak additional reflections are observed at approximately 28.3°, 30.3° and 55.7° for P1000, at 28.3° and 55.7° for P1050, and near 30.6° for P1100. The reflection near 28.3° is close to the Mn_3O_4 secondary-phase reflection reported at approximately 28.7° in $LaMnO_3$-based material [14] and is therefore tentatively attributed to a minor Mn_3O_4-related contribution. Residual Mn_3O_4 has also been reported as a secondary phase in thermally treated manganite perovskites [15]. The other weak reflections are treated as unresolved secondary contributions because their phase origin cannot be established confidently from the present diffraction data.

The number and prominence of these secondary reflections generally decrease with increasing sintering temperature, indicating improved development of the main $PrMnO_3$ phase. Among the samples investigated, P1100 shows the most favourable diffraction profile, with better-defined $PrMnO_3$ reflections and a lower secondary phase contribution than the samples sintered at lower temperatures.

https://doi.org/10.24191/srj.v23i2.58611

3.2 Rietveld and Structural Parameters

The structural stability of the perovskite framework was further evaluated using the Goldschmidt tolerance factor, τ as expressed in Eq. (2).

$$\tau = \frac{< r_A > + < r_o >}{\sqrt{2}(< r_B > + < r_o >)} \quad (2)$$

where r_A, r_B and r_0 are the ionic radii of the A-site cation, B-site cation and oxygen anion, respectively. The Goldschmidt tolerance factor provides an indication of structural distortion in a perovskite lattice. A value close to unity generally corresponds to an ideal cubic perovskite, whereas deviation from unity indicates distortion from the ideal cubic arrangement due to octahedral tilting and ionic size mismatch [16,17].

Table 1 presents the refined lattice parameters, unit-cell volume, Mn-O bond length, Mn-O-Mn bond angle, Goldschmidt tolerance factor and Rietveld refinement reliability factors for $PrMnO_3$ ceramics sintered at different temperatures. The refined lattice parameters confirm that all samples adopt an orthorhombic structure, where $a \neq b \neq c$. The unit-cell volume decreases from 233.76 Å^3 at 1000 °C to 232.88 Å^3 at 1050 °C, followed by a slight increase to 233.42 Å^3 at 1100 °C. This non-linear variation suggests that the lattice response is not governed only by simple thermal densification. Instead, it may involve local rearrangement of the MnO_6 octahedral network, variation in lattice strain and residual secondary contribution [3,8,18]. A different trend was reported by Teoh and Shamsuddin [11] for solid-state synthesised $Pr_{0.75}Na_{0.2}Ag_{0.05}MnO_3$, where the unit-cell volume decreased progressively from 229.8 Å^3 at 1100 °C to 229.1 Å^3 at 1200 °C. This difference suggests that the lattice response is not governed by sintering temperature alone and may also depend on composition, cation substitution and the processing range. Recent work on $PrMnO_3$-based manganites has similarly shown that Sr/Ba substitution modifies the degree of Jahn-Teller structural distortion [19].

Table 1. Refined lattice parameters, unit-cell volume, Mn-O bond lengths, Mn-O-Mn bond angles, Goldschmidt tolerance factor (τ), and Rietveld refinement reliability factors for $PrMnO_3$ ceramics sintered at different temperatures

Sample (°C)	Ts = 1000	Ts = 1050	Ts = 1100
Lattice parameter, Å			
a (Å)	5.5627	5.5476	5.5851
b (Å)	7.6946	7.6928	7.6605
c (Å)	5.4615	5.4568	5.4557
Volume, *V* (Å^3)	233.76	232.88	233.42
Bond distance, *d* <Mn-O> (Å)	1.9235	1.8400	1.8490
Bond angle, <Mn-O-Mn> (°)	155.09	161.00	156.70
R_p (%)	13.07	16.37	16.38
R_{wp} (%)	18.69	21.96	21.68
R_{exp} (%)	14.49	17.28	18.01
Goodness of fit, χ^2	1.680	1.628	1.463
Average ionic radii of A and O sites, <r*A*> + <r*o*>	3.1200	3.1200	3.1200
Average ionic radii of B and O sites, <r*B* > + <r*o*>	2.5900	2.5900	2.5900
Goldschmidt Tolerance factor, τ	0.8518	0.8518	0.8518

https://doi.org/10.24191/srj.v23i2.58611

The Mn-O bond length and Mn-O-Mn bond angle also vary with sintering temperature. The average Mn-O bond length decreases from 1.9235 Å at 1000 °C to 1.8400 Å at 1050 °C, before slightly increasing to 1.8490 Å at 1100 °C. Meanwhile, the Mn-O bond angle increases from 155.09° at 1000 °C to 161.00° at 1050 °C, followed by a decrease to 156.70° at 1100 °C. These changes indicate variation in the degree of MnO_6 octahedral distortion within the orthorhombic $PrMnO_3$ lattice. In perovskite manganites, the Mn-O bond distance and Mn-O-Mn bond angle are structurally important because they influence the tilting and connectivity of the MnO_6 octahedra [3]. Although no electrical or magnetic measurements are included in the present study, the observed bond-geometry variation provides useful structural information for future correlation with functional properties.

The Goldschmidt tolerance factor for all samples is 0.8518, reflecting the unchanged nominal composition of $PrMnO_3$ across the three sintering temperatures. This value is lower than the ideal cubic perovskite value of unity, indicating that the structure favours an orthorhombically distorted arrangement rather than a cubic perovskite lattice. Although the tolerance factor is composition-dependent, the effect of sintering temperature can be seen more clearly through the refined lattice parameters, unit-cell volume, Mn-O bond length, Mn-O-Mn bond angle and refinement reliability parameters.

Fig. 2 shows the final Rietveld refinement profiles of $PrMnO_3$ ceramics sintered at 1000 °C, 1050 °C and 1100 °C.

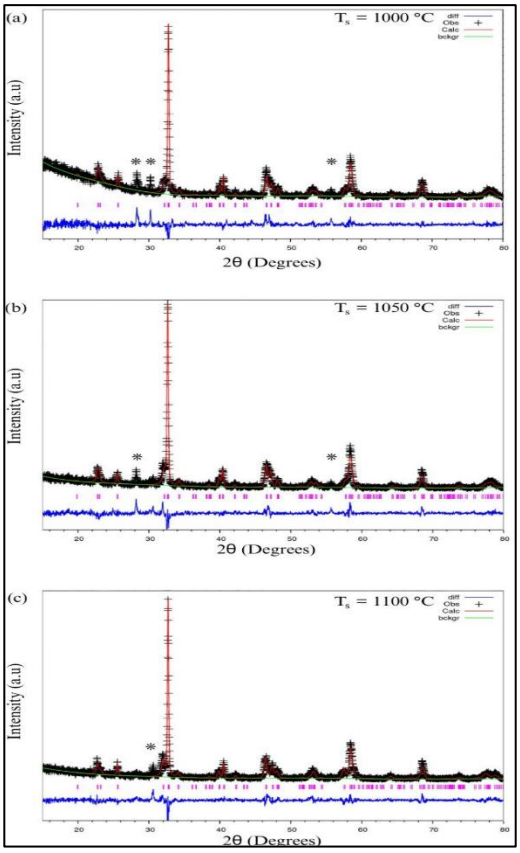

Fig. 2. Final Rietveld refinement profiles of $PrMnO_3$ ceramics sintered at (a) 1000 °C, (b) 1050 °C and (c) 1100 °C

https://doi.org/10.24191/srj.v23i2.58611

The observed and calculated profiles show reasonable agreement for all samples, as supported by the refinement reliability parameters listed in Table 1. The R_p, R_{wp} and R_{exp} values complement the χ^2 value in assessing the agreement between the observed and calculated diffraction profiles. The Bragg peak positions correspond to the orthorhombic *Pnma* phase, confirming that the structural model is suitable for describing the main $PrMnO_3$ phase. The refinement analysis was conducted using GSAS/EXPGUI and visualised using VESTA, which are widely used for crystallographic refinement and structural visualisation [12,13,20].

The difference curves in Fig. 2 show that the largest deviations occur around the intense diffraction peaks. These deviations may arise from small differences between the measured and calculated peak intensities, peak widths, preferred orientation or background contribution. Weak secondary reflections, including the feature tentatively associated with a minor Mn_3O_4-related contribution, are indicated by asterisks in the refinement profiles. These features are more noticeable for the sample sintered at 1000 °C and become less pronounced with increasing sintering temperature. This supports the interpretation that higher sintering temperature improves reaction completeness and reduces secondary phase contribution.

The refinement reliability factors show some variation among the three samples. R_p increases from 13.07% for P1000 to 16.37% for P1050 and remains nearly unchanged at 16.38% for P1100, while R_{wp} varies from 18.69% to 21.96% and 21.68%, respectively. R_{exp} increases from 14.49% to 17.28% and 18.01%. Thus, the profile residuals do not show a monotonic improvement with sintering temperature. In contrast, χ^2 decreases from 1.680 for P1000 to 1.628 for P1050 and 1.463 for P1100. Taken together, these parameters indicate acceptable agreement between the observed and calculated profiles, with P1100 giving the lowest χ^2 among the three refinements. Within the investigated temperatures, the 1100 °C sample shows the most favourable structural development, with the lowest χ^2 value and a reduced contribution from weak secondary reflection.

3.3 SEM-EDX Analysis

Fig. 3 shows the SEM micrographs of $PrMnO_3$ ceramics sintered at 1000 °C, 1050 °C and 1100 °C. The sample sintered at 1000 °C exhibits relatively fine and loosely packed grains with visible intergranular pores. This morphology indicates that the ceramic body is not fully densified at this temperature. The observation is consistent with the XRD and Rietveld results, where the 1000 °C sample shows less-developed diffraction features and a higher χ^2 value.

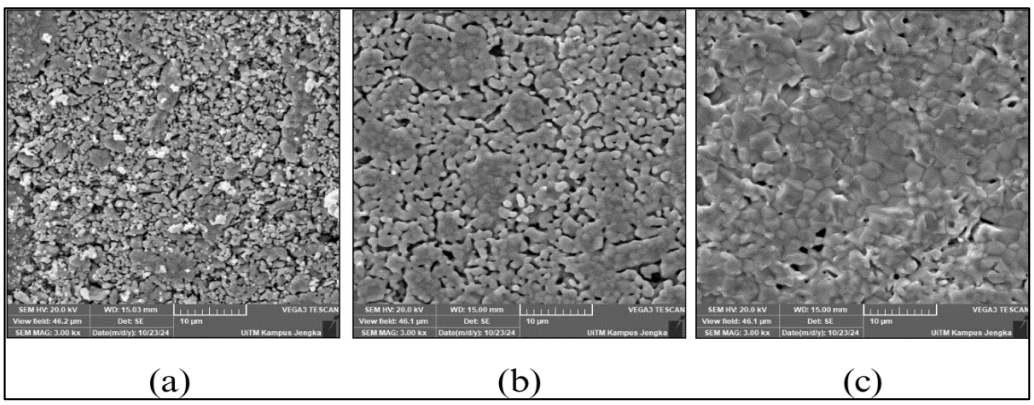

Fig. 3. SEM micrographs of $PrMnO_3$ ceramics sintered at (a) 1000 °C, (b) 1050 °C and (c) 1100 °C

https://doi.org/10.24191/srj.v23i2.58611

At 1050 °C, the grains become more connected, and the pore distribution appears reduced compared with the 1000 °C sample. This suggests improved intergranular contact and partial densification. For the sample sintered at 1100 °C, the microstructure becomes more compact, with clearer grain boundaries and lower intergranular porosity. This indicates that higher sintering temperature enhances densification and grain development. A similar microstructural trend was reported by Keshvani et al. [10] for undoped sol-gel-derived $PrMnO_3$, where increasing sintering temperature produced larger grains with sharper boundaries and reduced porosity. Teoh and Shamsuddin [11] also observed improved grain connectivity, increased densification and reduced porosity in solid-state-synthesised Na/Ag-doped Pr-based manganite at 1100-1200 °C. The agreement with the present observations suggests that grain growth and densification are common thermally activated features of Pr-based manganites, although their detailed structural response may vary with composition and processing route.

The SEM results support the XRD and Rietveld refinement findings. The improved compactness observed at 1100 °C corresponds well with the better-defined diffraction peaks and lower χ^2 value obtained from refinement analysis. Therefore, the morphological evidence confirms that the sintering temperature plays an important role not only in the phase formation but also in the microstructural development of undoped $PrMnO_3$ ceramics.

Fig. 4 shows the EDX spectra of $PrMnO_3$ ceramics sintered at 1000 °C, 1050 °C and 1100 °C, and the corresponding elemental compositions are listed in Table 2. The spectra show the presence of Pr, Mn and O in all samples, which is consistent with the expected Pr-Mn-O ceramic composition. No obvious foreign elemental peaks are detected, suggesting that no major contamination occurred during the process. As expected, Pr gives the highest weight percentage due to its larger atomic mass compared with Mn and O.

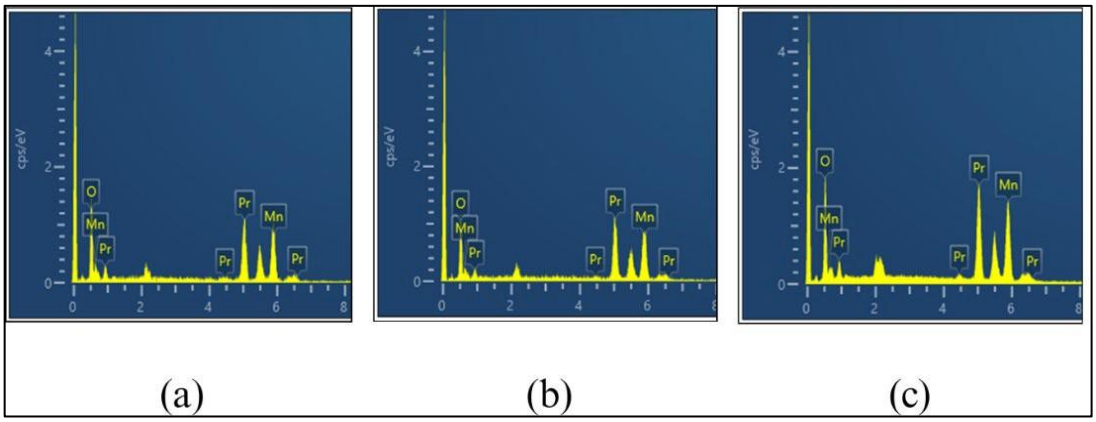

Fig. 4. EDX spectra of $PrMnO_3$ ceramics sintered at temperatures, Ts, of (a) 1000 °C, (b) 1050 °C and (c) 1100 °C, confirming the presence of Pr, Mn and O as the main constituent elements

https://doi.org/10.24191/srj.v23i2.58611

Table 2. Weight and atomic percentages of Pr, Mn, and O obtained from EDX analysis for $PrMnO_3$ ceramics sintered at different temperatures

Element	**Pr**		**Mn**		**O**	
Samples (°C)	Weight (%)	Atomic (%)	Weight (%)	Atomic (%)	Weight (%)	Atomic (%)
T_s = 1000	54.1	16.53	21.0	16.42	24.9	67.05
T_s = 1050	58.1	19.43	20.6	17.70	21.3	62.87
T_s = 1100	57.7	18.79	19.8	16.58	22.5	64.63

The Pr and Mn atomic percentages are reasonably close across the three samples, indicating that the cationic composition remains broadly consistent with the intended $PrMnO_3$-based system. The oxygen content, however, is treated as a semi-quantitative value because EDX analysis is generally less reliable for light elements and may be influenced by surface condition, interaction volume and sample roughness [21]. Therefore, the EDX results are used mainly to support the elemental presence of Pr, Mn and O, rather than to confirm exact stoichiometry.

In relation to phase formation, the EDX results should be interpreted together with the XRD and Rietveld refinement analysis. This is because possible minor oxide-related phases may contain elements already present in the main Pr-Mn-O system and may not be clearly distinguished by EDX alone. Thus, the role of EDX in this study is to provide supporting compositional evidence, while the identification of the main phase and minor secondary contributions is based primarily on the diffraction analysis.

3.4 Structural –Morphological Correlation

The structural and morphological results show a consistent effect of sintering temperature on the development of undoped $PrMnO_3$ ceramics. The improvement in diffraction peak definition, lower χ^2 value and reduced weak secondary reflections at higher sintering temperature are in line with the SEM observation, where the microstructure becomes more compact and less porous. This suggests that higher thermal treatment promotes better reaction progress, crystallographic ordering and grain connectivity.

Among the temperatures studied, 1100 °C shows the most favourable structural and morphological development, supported by its better-developed diffraction profile, lower secondary-phase contribution and denser microstructure. Although weak secondary contributions are still present, the combined XRD, Rietveld-refinement and SEM results indicate improved structural and microstructural development at 1100 °C compared with lower sintering temperatures. This interpretation is limited to the structural and morphological properties examined in the present study.

4. CONCLUSION

Undoped $PrMnO_3$ perovskite manganite ceramics were prepared using the conventional solid-state method and sintered at 1000 °C, 1050 °C and 1100 °C. XRD and Rietveld refinement analyses confirmed the formation of the main orthorhombic perovskite-related $PrMnO_3$ structure with *Pnma* symmetry. Weak additional reflections were observed, particularly at lower sintering temperatures, but their number and prominence generally decreased with increasing sintering temperature, indicating improved formation of

https://doi.org/10.24191/srj.v23i2.58611

the main $PrMnO_3$ phase. The refinement results showed that the χ^2 value decreased from 1.680 at 1000 °C to 1.463 at 1100 °C, while slight variations in lattice parameters, unit-cell volume and Mn-O bond geometry reflected changes in the orthorhombic lattice arrangement. SEM analysis further showed densification and reduced intergranular porosity at higher sintering temperatures, while EDX confirmed the presence of Pr, Mn and O as the main constituent elements. Overall, the sample sintered at 1100 °C showed the most favourable structural and morphological development among the investigated temperatures. This conclusion is limited to the structural and morphological characteristics evaluated in the present study.

5. ACKNOWLEDGEMENTS/FUNDING

The authors would like to acknowledge the Faculty of Applied Sciences, Universiti Teknologi MARA (UiTM), Pahang Branch, Jengka Campus, and UiTM Shah Alam, for providing the laboratory facilities and research support for this work. The authors also acknowledge the technical assistance provided during the sample preparation and characterization. This research did not receive any specific grant from public, commercial or not-for-profit funding agencies.

6. CONFLICT OF INTEREST STATEMENT

The authors agree that this research was conducted in the absence of any self-benefits, commercial or financial conflicts and declare the absence of conflicting interests.

7. AUTHORS' CONTRIBUTIONS

Muhamad Fauzan Fakhri Mohamad: Methodology, investigation, formal analysis, data curation and visualisation; Nur Baizura Mohamed: Conceptualisation, methodology, validation, supervision, project administration, writing-original draft, writing-review and editing; Rozilah Rajmi: Validation, formal analysis and supervision; Zakiah Mohamed: Resources and validation; Siti Aishah Abdul Aziz: Writing-review and editing.

8. DECLARATION OF GENERATIVE AI IN THE WRITING PROCESS

During the preparation of this work, the author(s) used ChatGPT to improve the readability, language quality and structural clarity of the manuscript. After using this tool, the author(s) reviewed and edited the content as needed and take full responsibility for the content, accuracy and integrity of the publication.

9. DATA AVAILABILITY/SUPPLEMENTARY MATERIALS

The datasets used and/or analysed during the current study are available from the corresponding author upon reasonable request.

10. ETHICS STATEMENT

The authors declare that this research did not involve human or animal subjects. All experimental procedures were performed following the institutional Safety, Health and Environmental protocols of Universiti Teknologi MARA.

11. REFERENCES

[1] C. J. Aguilar, E. Mosquera, F. Gracia, J. E. Diosa & J. E. Rodríguez-Páez, 2022. $PrMnO_3$ porous nanostructures: Synthesis and structural, optical and magnetic properties. *Materials Research Bulletin*, 151, 111805. DOI: 10.1016/j.materresbull.2022.111805.

[2] G. George, S. R. Ede & Z. Luo, 2020. *Fundamentals of Perovskite oxides: Synthesis, structure, properties and applications*, CRC Press. DOI: 10.1201/9780429351419.

[3] P. G. Radaelli, G. Iannone, M. Marezio, H. Y. Hwang, S.-W. Cheong, J. D. Jorgensen & D. N. Argyriou, 1997. Structural effects on the magnetic and transport properties of perovskite $A_{1-x}A'_xMnO_3$ (x = 0.25, 0.30). *Physical Review B*, 56(13), 8265-8276. DOI: 10.1103/PhysRevB.56.8265.

[4] S. Kumari, R. Rai, P. Kumar, O. P. Thakur & R. Chatterjee, 2022. The effect of Eu dopant on the structural, dielectric and impedance properties of $PrMnO_3$ manganite ceramics. *Journal of Physics and Chemistry of Solids*, 160, 110365. DOI: 10.1016/j.jpcs.2021.110365.

[5] R. Rozilah, N. Ibrahim & A. K. Yahya, 2019. Inducement of ferromagnetic-metallic phase and magnetoresistance behavior in charged ordered monovalent-doped $Pr_{0.75}Na_{0.25}MnO_3$ manganite by Ni substitution. *Solid State Sciences*, 87, 64-80. DOI: 10.1016/j.solidstatesciences.2018.11.005.

[6] A. Sajawal, M. Ishfaq, G. Murtaza, I. Habib, N. Muhammad & S. Sharif, 2018. Half metallic ferromagnetism in $PrMnO_3$ orthorhombic stable phase: An experimental and theoretical investigation. *Materials Research Express*, 5(11), 116103. DOI: 10.1088/2053-1591/aade7d.

[7] M. Arunachalam, P. Thamilmaran & K. Sakthipandi, 2020. Effect of sintering temperature on metal-insulator phase transition in $La_{1-x}Ca_xMnO_3$ perovskites. *Frontiers in Advanced Materials Research*, 2(1), 37-42. DOI: 10.34256/famr2014.

[8] Y. Liu, T. Sun, G. Dong, S. Zhang, K. Chu, X. Pu, H. Li & X. Liu, 2019. Dependence on sintering temperature of structure, optical and magnetic properties of $La_{0.625}Ca_{0.315}Sr_{0.06}MnO_3$ perovskite nanoparticles. *Ceramics International*, 45(14), 17467-17475. DOI: 10.1016/j.ceramint.2019.05.308.

[9] A. E. Irmak, A. Coskun, E. Tasarkuyu, S. Akturk, G. Unlu, Y. Samancioglu, C. Sarikurkcu, B. M. Kaynar & A. Yucel, 2010. The influence of the sintering temperature on the structural and the magnetic properties of doped manganites: $La_{0.95}Ag_{0.05}MnO_3$ and $La_{0.75}Ag_{0.25}MnO_3$. *Journal of Magnetism and Magnetic Materials*, 322(8), 945-951. DOI: 10.1016/j.jmmm.2009.11.029.

[10] M. J. Keshvani, S. Katba, S. Jethva, M. Udeshi, B. Kataria, A. Ravalia & D. G. Kuberkar, 2017. Studies on structural, morphological and electroresistance properties of sol-gel grown nanostructured $PrMnO_3$. *Materials Science and Engineering: B*, 218, 40-50. DOI: 10.1016/j.mseb.2017.02.006.

[11] W. W. Teoh & S. Shamsuddin, 2022. Effect of sintering temperature on structural and surface morphology of manganite: $Pr_{0.75}Na_{0.25-x}Ag_xMnO_3$. *Enhanced Knowledge in Sciences and Technology*, 2(2), 52-59. DOI: 10.30880/ekst.2022.02.02.006.

[12] A. C. Larson & R. B. Von Dreele, 2004. *General Structure Analysis System (GSAS)* (Los Alamos National Laboratory Report LAUR 86-748). Los Alamos National Laboratory.

[13] B. H. Toby, 2001. EXPGUI, a graphical user interface for GSAS. *Journal of Applied Crystallography*, 34(2), 210-213. DOI: 10.1107/S0021889801002242.

[14] N. Özbay & R. Z. Yarbay Şahin, 2017. Preparation and characterization of $LaMnO_3$ and $LaNiO_3$ perovskite type oxides by the hydrothermal synthesis method. *AIP Conference Proceedings*, 1809, 020040. DOI: 10.1063/1.4975455.

[15] N. El Hamouchi, S. Ait Bouzid, M. Sajieddine, E. K. Hlil, M. Mansori & A. Essoumhi, 2026. Effect of sintering conditions on the structure, microstructure, magnetic, and magnetocaloric properties of $La_{0.8}Na_{0.2}MnO_3$. *Applied Physics A*, 132, 536. DOI: 10.1007/s00339-026-09700-1.

[16] R. D. Shannon, 1976. Revised effective ionic radii and systematic studies of interatomic distances in halides and chalcogenides. *Acta Crystallographica Section A*, 32(5), 751-767. DOI: 10.1107/S0567739476001551.

[17] V. M. Goldschmidt, 1926. Die Gesetze der Krystallochemie. *Naturwissenschaften*, 14, 477-485. DOI: 10.1007/BF01507527.

[18] D. S. Razaq, D. R. Munazat, B. Soegijono, B. Kurniawan, S. Budiawanti & D. Nanto, 2020. Effect of sintering temperature on the structural properties of La0.7Sr0.25Nd0.05MnO3. In *Proceedings of the 2nd International Conference on Quran and Hadith Studies Information Technology and Media in Conjunction with the 1st International Conference on Islam, Science and Technology*. EAI. DOI: 10.4108/eai.2-10-2018.2295450.

[19] L. Vedmid', O. Fedorova, A. Fetisov, E. Konysheva & S. Uporov, 2024. Influence of low-level substitution Pr/(Sr or Ba) in $PrMnO_3$ on structure distortions, magnetic transitions, and surface evolution. *Journal of Materials Science: Materials in Electronics*, 35, 1369. DOI: 10.1007/s10854-024-13152-9.

[20] K. Momma & F. Izumi, 2011. VESTA 3 for three-dimensional visualization of crystal, volumetric and morphology data. *Journal of Applied Crystallography*, 44(6), 1272-1276. DOI: 10.1107/S0021889811038970.

[21] J. I. Goldstein, D. E. Newbury, J. R. Michael, N. W. M. Ritchie, J. H. J. Scott & D. C. Joy, 2018. *Scanning electron microscopy and X-ray microanalysis* (4th ed.). Springer. DOI: 10.1007/978-1-4939-6676-9.